

Advancing Graph Generation through Beta Diffusion

Yilin He^{1,*}, Xinyang Liu^{2,*}, Bo Chen², and Mingyuan Zhou¹

yilin.he@mcombs.utexas.edu, xinyangatk@gmail.com
bchen@mail.xidian.edu.cn, mingyuan.zhou@mcombs.utexas.edu

¹The University of Texas at Austin, ²Xidian University

Abstract

Diffusion models have demonstrated effectiveness in generating natural images and have been extended to generate diverse data types, including graphs. This new generation of diffusion-based graph generative models has demonstrated significant performance improvements over methods that rely on variational autoencoders or generative adversarial networks. It’s important to recognize, however, that most of these models employ Gaussian or categorical diffusion processes, which can struggle with sparse and long-tailed data distributions. In our work, we introduce Graph Beta Diffusion (GBD), a diffusion-based generative model particularly adept at capturing diverse graph structures. GBD utilizes a beta diffusion process, tailored for the sparse and range-bounded characteristics of graph adjacency matrices. Furthermore, we have developed a modulation technique that enhances the realism of the generated graphs by stabilizing the generation of critical graph structures, while preserving flexibility elsewhere. The outstanding performance of GBD across three general graph benchmarks and two biochemical graph benchmarks highlights its capability to effectively capture the complexities of real-world graph data. The code will be made available on GitHub. The code will be made available at https://github.com/YH-UtMSB/Graph_Beta_Diffusion.

1 Introduction

In recent years, the field of machine learning-driven graph generation has witnessed a surge in interest and activity. This growing attention is driven by the recognition of graph data’s pervasive presence and utility across diverse real-world applications, ranging from social network study [Newman et al., 2002, Conti et al., 2011, Abbe, 2018, Shirzadian et al., 2023] to biochemical molecular research [Jin et al., 2018, Liu et al., 2018, Bongini et al., 2021, Guo et al., 2024, Li and Yamanishi, 2024]. Additionally, the rapid evolution of machine learning tools has introduced powerful techniques for data generation, among which diffusion models [Ho et al., 2020, Song et al., 2021, Austin et al., 2021, Avdeyev et al., 2023, Chen and Zhou, 2023, Zhou et al., 2023] stand out as a notable example. As these advanced tools intersect with the task of graph generation, we witness the emergence of numerous diffusion-based graph generative models [Niu et al., 2020a, Jo et al., 2022, Haefeli et al., 2022, Huang et al., 2022, Vignac et al., 2023, Jo et al., 2023, Cho et al., 2023, Chen et al., 2023, Kong et al., 2023].

While diffusion-based graph generative models often demonstrate superior performance compared to their predecessors [You et al., 2018, De Cao and Kipf, 2018, Li et al., 2018, Simonovsky and Komodakis, 2018, Liu et al., 2019, Shi et al., 2020, Luo et al., 2021, Martinkus et al., 2022], there is still potential for further enhancement in the quality of generated graphs. Among the latest advancements in these methods, it is widely recognized that incorporating inductive bias from the graph data is generally beneficial for model design [Jo et al., 2023]. One promising direction of incorporating this bias involves considering the statistical

*The first two authors contribute equally.

characteristics of the distribution of graph data. For instance, both Graph D3PM [Haefeli et al., 2022] and DiGress [Vignac et al., 2023] have demonstrated that when considering the binary or categorical nature of the graph adjacency matrix and modeling it in the discrete space, it provides benefits for generating more realistic graphs.

Accounting for the discreteness of the graph adjacency matrix has shown enhancement to model performance. However, it is crucial to recognize that the complexity and flexibility of distribution characteristics of graph data extend beyond mere discreteness. Real-world graphs typically exhibit sparsity in edge distribution and long-tailedness in nodal statistical properties such as degrees and categories [Barabási et al., 2000, Ciotti et al., 2015, Liang et al., 2023, Wang et al., 2023]. Moreover, when mapping the graph structure into an adjacency matrix, the values within the matrix are also bounded by the range of edge weights. Given these unique characteristics inherent to graph data, it becomes apparent that Gaussian and categorical distributions, which are typically the default choices for building the diffusion processes, may not align well with these graph characteristics. Consequently, this mismatch could potentially introduce limitations when modeling the distribution over graphs.

Considering the desirable statistical characteristics of graph data, we find that the beta distribution emerges as a particularly suitable modeling choice. With properties such as being range-bounded and flexible to model data at all sparsity levels, the beta distribution aligns well with the inherent traits of graphs, hence making itself a promising candidate to surpass the potential limitations imposed by utilizing Gaussian or categorical distributions. In this paper, we introduce Graph Beta Diffusion (GBD) as a novel addition to diffusion-based graph generative models. GBD models the joint distribution of node attributes and edge connections within a graph through beta diffusion [Zhou et al., 2023], a generative diffusion process developed upon the thinning and thickening of beta random variables. In the forward diffusion process, the original data is gradually attenuated toward zero. This process starts with a modified form of the data, which is scaled and shifted to ensure it is bounded between 0 and 1. At each step, a random proportion, sampled from a beta distribution with a predefined noise schedule, is multiplied with the attenuated data. Conversely, the reverse diffusion process starts from zero and attempts to recover the original data. It does this by adding a random proportion of the difference between one and the current value to the current value at each step.

We underscore two major contributions arising from the development of GBD. First, our experiments generating data on various synthetic and real-world graphs confirm the effectiveness of beta diffusion as a strategic choice within the design framework of the backbone diffusion model, especially for graph generation tasks. Second, our exploration of the model’s design space has yielded a set of recommended practices, notably a novel modulation technique that bolsters the stability of generating essential graph structures. We demonstrate that these practices, when implemented together, lead to consistent enhancements in model performance.

2 The Methodology

2.1 Data description and mathematical notations

In this study, our primary focus lies in generating two types of graphs: generic graphs and molecular graphs. Generic graphs are characterized as undirected, simple graphs with N nodes. Each pair of nodes (u, v) in these graphs can only have two possible edge statuses: connected or disconnected. Therefore, the entire graph structure can be fully described by a symmetric binary adjacency matrix $\mathbf{A} \in \{0, 1\}^{n \times n}$, where “1”s denote connected node pairs and “0”s denote pairs that are not directly connected. Molecular graphs are also simple graphs, but they typically feature multiple types of edges. As a result, their graph structures need to be represented as adjacency matrices with dummy-encoded categorical variable elements, which is a common practice established in previous research [Jo et al., 2022, Vignac et al., 2023, Jo et al., 2023]. This expression results in a multitude of channels in the graph adjacency matrix, we use $\mathbf{A}^{(1:K)}$ to represent the structure of a graph with K types of edges.

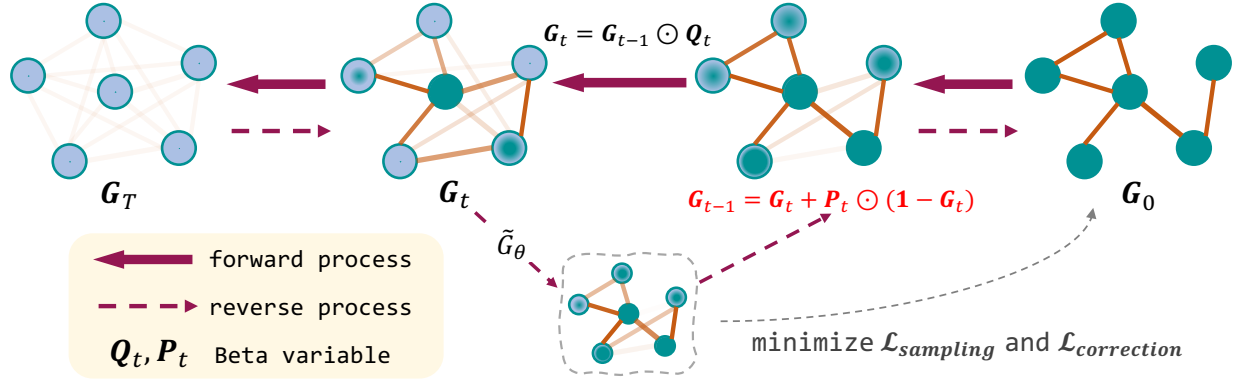


Figure 1: Overview of GBD. The beta random variables Q_t and P_t are sampled from the beta distribution parameterized by G_0 and clean graph predicted by the neural network \tilde{G}_θ , respectively. \tilde{G}_θ is learned through minimizing $\mathcal{L}_{\text{sampling}}$ and $\mathcal{L}_{\text{correction}}$ defined in Section 2.3.

While the primary goal of graph generation and quality evaluation centers around graph architecture, incorporating the node features can be advantageous for learning the distribution of the adjacency matrices. Node features are typically represented by a matrix \mathbf{X} of shape $n \times d$, where d denotes the number of features. The choices of node features offers high flexibility, ranging from raw-data-provided node categories to some hand-crafted features, such as node-level statistics [Jo et al., 2022] or spectral graph signals [Jo et al., 2023]. The features within \mathbf{X} exhibit great diversity in their nature, including numerical, categorical, and ordinal types. Through preprocessing methods including dummy-encoding and empirical CDF transformation, we standardize them as continuous variables bounded by $[0, 1]$. In this section, we denote the target datum as \mathbf{G} . For generic graphs, \mathbf{G} comprises (\mathbf{A}, \mathbf{X}) ; for molecular graphs, \mathbf{G} is defined as $(\mathbf{A}^{(1:K)}, \mathbf{X})$. In the sequel, We by default employ the generic graph scenario to illustrate the methodology.

2.2 Forward and reverse beta diffusion processes

Forward beta diffusion process. Such a process can be characterized by the transition probability $q(\mathbf{G}_t | \mathbf{G}_{t-1}, \mathbf{G}_0)$, with \mathbf{G}_0 denoting the combination of the original adjacency matrix and node feature matrix. Following recent diffusion-based graph generative models [Jo et al., 2022, Vignac et al., 2023, Jo et al., 2023, Cho et al., 2023], we assume $q(\mathbf{G}_t | \mathbf{G}_{t-1}, \mathbf{G}_0)$ to be factorizable such that $q(\mathbf{G}_t | \mathbf{G}_{t-1}, \mathbf{G}_0) = q(\mathbf{A}_t | \mathbf{A}_{t-1}, \mathbf{A}_0) \cdot q(\mathbf{X}_t | \mathbf{X}_{t-1}, \mathbf{X}_0)$. Constructing the forward beta diffusion process [Zhou et al., 2023] for graph modeling, we have:

$$\mathbf{A}_t = \mathbf{A}_{t-1} \odot \mathbf{Q}_{A,t}, \quad \mathbf{Q}_{A,t} \sim \text{Beta}(\eta_A \alpha_t \mathbf{A}_0, \eta_A (\alpha_{t-1} - \alpha_t) \mathbf{A}_0), \quad (1)$$

$$\mathbf{X}_t = \mathbf{X}_{t-1} \odot \mathbf{Q}_{X,t}, \quad \mathbf{Q}_{X,t} \sim \text{Beta}(\eta_X \alpha_t \mathbf{X}_0, \eta_X (\alpha_{t-1} - \alpha_t) \mathbf{X}_0), \quad t \in [1, T]. \quad (2)$$

Here η_A, η_X are positive scalars adjusting the concentration of beta distributions, with higher values leading to enhanced concentration and reduced variability. The diffusion noise schedule is defined with $\{\alpha_t \mid t \in [1, T]\}$, which represent a sequence of values descending from 1 towards 0 as t increases. Elements in the fractional multiplier $\mathbf{Q}_{A,t}$ or $\mathbf{Q}_{X,t}$ are independently sampled from their respective beta distributions. With the forward diffusion process defined in Equations (1) and (2), we characterize the stochastic transitions of an element g within \mathbf{G} as:

$$q(g_t \mid g_{t-1}, g_0) = \frac{1}{g_{t-1}} \text{Beta}\left(\frac{g_t}{g_{t-1}} \mid \eta \alpha_t g_0, \eta (\alpha_{t-1} - \alpha_t) g_0\right), \quad (3)$$

where depending on whether g is an element in \mathbf{A} or \mathbf{X} , we have either $\eta = \eta_A$ or $\eta = \eta_X$. Derived from Equation (3), the joint distribution $q(\mathbf{G}_{1:T} | \mathbf{G}_0)$ has analytical format in the marginal distribution on each time stamp t , specifically,

$$q(\mathbf{G}_t \mid \mathbf{G}_0) = \text{Beta}(\eta \alpha_t \mathbf{G}_0, \eta (1 - \alpha_t) \mathbf{G}_0). \quad (4)$$

Reverse beta diffusion process. It is important to note that the joint distribution $q(\mathbf{G}_{1:T}|\mathbf{G}_0)$ can be equivalently constructed in reverse order through ancestral sampling, which directs samples from the terminus states \mathbf{G}_T towards the initial states \mathbf{G}_0 by incrementally applying the changes $\delta\mathbf{G}_t$ at each reversed time stamp. With the changes at a given time t parameterized as $\delta\mathbf{G}_t := \mathbf{P}_t \odot (1 - \mathbf{G}_t)$, where \mathbf{P}_t are beta-distributed fractional multipliers, the time-reversal sampling process can be mathematically defined as: for $t = T, T - 1, \dots, 1$,

$$\mathbf{G}_{t-1} = \mathbf{G}_t + \mathbf{P}_t \odot (1 - \mathbf{G}_t), \mathbf{P}_t \sim \text{Beta}(\eta(\alpha_{t-1} - \alpha_t)\mathbf{G}_0, \eta(1 - \alpha_t\mathbf{G}_0)). \quad (5)$$

Similar to the forward sampling process, we can derive the transition distribution corresponding to the reverse sampling process described in Equation (5) as following:

$$q(\mathbf{G}_{t-1} | \mathbf{G}_t, \mathbf{G}_0) = \frac{1}{1 - \mathbf{G}_t} \text{Beta}\left(\frac{\mathbf{G}_{t-1} - \mathbf{G}_t}{1 - \mathbf{G}_t} \mid \eta(\alpha_{t-1} - \alpha_t)\mathbf{G}_0, \eta(1 - \alpha_{t-1}\mathbf{G}_0)\right). \quad (6)$$

Following previous work [Austin et al., 2021, Haefeli et al., 2022, Vignac et al., 2023, Zhou et al., 2023], we construct the reverse diffusion process through the definition of ancestral sampling distribution as following:

$$p_\theta(\mathbf{G}_{t-1} | \mathbf{G}_t) := q(\mathbf{G}_{t-1} | \mathbf{G}_t, \hat{\mathbf{G}}_\theta(\mathbf{G}_t, t)), \quad (7)$$

where $\hat{\mathbf{G}}_\theta(\mathbf{G}_t, t)$ is a neural network that predicts the conditional expectation of \mathbf{G}_0 given \mathbf{G}_t . Following Vignac et al. [2023], we instantiate $\hat{\mathbf{G}}_\theta(\mathbf{G}_t, t)$ as a graph transformer network [Dwivedi and Bresson, 2020a]. We present the complete sampling process in Algorithms 1 and 2.

Algorithm 1 Sampling, in original domain.

Require: Number of timesteps $T = 1000$, default concentration parameter $\eta = 30$, predictor $\hat{\mathbf{G}}_\theta$.

- 1: (Optional) Assign value to η via Equation (16)
- 2: Sample $\mathbf{G}_T = (\mathbf{A}_T, \mathbf{X}_T) \sim p(\mathbf{A}_T, \mathbf{X}_T)$
- 3: **for** $t = T$ to 1 **do**
- 4: $\mathbf{G}_{in} = \frac{\mathbf{G}_t - \mathbb{E}[\mathbf{G}_t]}{\sqrt{\text{Var}[\mathbf{G}_t]}}$
- 5: $(\hat{\mathbf{A}}'_0, \hat{\mathbf{X}}'_0) \leftarrow \hat{\mathbf{G}}_\theta(\mathbf{G}_{in}, t)$
- 6: $\hat{\mathbf{A}}_0 \leftarrow w_A \cdot \hat{\mathbf{A}}'_0 + b_A$
- 7: $\hat{\mathbf{X}}_0 \leftarrow w_X \cdot \hat{\mathbf{X}}'_0 + b_X$
- 8: $\hat{\mathbf{G}}_0 \leftarrow (\hat{\mathbf{A}}_0, \hat{\mathbf{X}}_0)$
- 9: $\mathbf{P}_t \sim \text{Beta}(\eta(\alpha_{t-1} - \alpha_t)\hat{\mathbf{G}}_0, \eta(1 - \alpha_{t-1}\hat{\mathbf{G}}_0))$
- 10: $\mathbf{G}_{t-1} \leftarrow \mathbf{G}_t + \mathbf{P}_t \odot (1 - \mathbf{G}_t)$
- 11: **end for**
- 12: **return** $(\mathbf{A}_0 - b_A)/w_A$ and $(\mathbf{X}_0 - b_X)/w_X$

Algorithm 2 Sampling, in logit domain

- 1: Sample $\text{logit}(\mathbf{G}_T) \sim p(\text{logit}(\mathbf{A}_T), \text{logit}(\mathbf{X}_T))$
- 2: **for** $t = 1$ to 1 **do**
- 3: $\mathbf{G}_{in} = \frac{\text{logit}(\mathbf{G}_t) - \mathbb{E}[\text{logit}(\mathbf{G}_t)]}{\sqrt{\text{Var}[\text{logit}(\mathbf{G}_t)]}}$
- 4: $(\hat{\mathbf{A}}'_0, \hat{\mathbf{X}}'_0) \leftarrow \hat{\mathbf{G}}_\theta(\mathbf{G}_{in}, t)$
- 5: $\hat{\mathbf{A}}_0 \leftarrow w_A \cdot \hat{\mathbf{A}}'_0 + b_A$
- 6: $\hat{\mathbf{X}}_0 \leftarrow w_X \cdot \hat{\mathbf{X}}'_0 + b_X$
- 7: $\hat{\mathbf{G}}_0 \leftarrow (\hat{\mathbf{A}}_0, \hat{\mathbf{X}}_0)$
- 8: $\mathbf{U}_t \sim \text{Gamma}(\eta(\alpha_{t-1} - \alpha_t)\hat{\mathbf{G}}_0, 1)$
- 9: $\mathbf{V}_t \sim \text{Gamma}(\eta(1 - \alpha_{t-1}\hat{\mathbf{G}}_0), 1)$
- 10: $\text{logit}(\mathbf{P}_t) \leftarrow \ln \mathbf{U}_t - \ln \mathbf{V}_t$
- 11: Obtain $\text{logit}(\mathbf{G}_{t-1})$ from Equation (17)
- 12: **end for**
- 13: $\mathbf{G}_0 \leftarrow \text{sigmoid}(\text{logit}(\mathbf{G}_0))$
- 14: **return** $(\mathbf{A}_0 - b_A)/w_A$ and $(\mathbf{X}_0 - b_X)/w_X$

2.3 Training GBD

The overall training procedure of GBD is described in Algorithms 3 and 4. We employ the objective function proposed by beta diffusion [Zhou et al., 2023], specifically,

$$\mathcal{L} = \sum_{t=2}^T (1 - \omega)\mathcal{L}_{\text{sampling}}(t, \mathbf{G}_0) + \omega \mathcal{L}_{\text{correction}}(t, \mathbf{G}_t), \omega \in [0, 1]. \quad (8)$$

In Equation (8), the loss terms associated with sampling and correction are defined as

$$\mathcal{L}_{\text{sampling}}(t, \mathbf{G}_0) \triangleq \mathbb{E}_{q(\mathbf{G}_t, \mathbf{G}_0)} \text{KL}(p_\theta(\mathbf{G}_{t-1} | \mathbf{G}_t) \parallel q(\mathbf{G}_{t-1} | \mathbf{G}_t, \mathbf{G}_0)), \quad (9)$$

$$\mathcal{L}_{\text{correction}}(t, \mathbf{G}_0) \triangleq \mathbb{E}_{q(\mathbf{G}_t, \mathbf{G}_0)} \text{KL}\left(q(\mathbf{G}_T | \hat{\mathbf{G}}_\theta(\mathbf{G}_t, t)) \parallel q(\mathbf{G}_T | \mathbf{G}_0)\right). \quad (10)$$

In Equation (10), the KL divergence is evaluated between the following distributions: $q(\mathbf{G}_\tau | \hat{G}_\theta(\mathbf{G}_t, t))$ is $\text{Beta}(\eta\alpha_t\hat{G}_\theta(\mathbf{G}_t, t), \eta(1 - \alpha_t\hat{G}_\theta(\mathbf{G}_t, t)))$, and $q(\mathbf{G}_\tau | \mathbf{G}_0)$ is the same as $q(\mathbf{G}_t | \mathbf{G}_0)$ in distribution. The subscript τ is introduced to represent a generic graph sample other than \mathbf{G}_t that is also obtained at time t from the forward diffusion process. The core principle behind the loss function terms can be described as follows: $\mathcal{L}_{\text{sampling}}$ drives the empirical ancestral sampling distribution towards the destination-conditional posterior distribution, while $\mathcal{L}_{\text{correction}}$ corrects the bias on marginal distribution at each time stamp accumulated through the ancestral sampling. These two types of loss terms collectively reduce the divergence between the empirical joint distribution on two graphs sampled from adjacent time stamps in the reverse process, and their joint distribution derived from the forward diffusion process. A positive weight ω is introduced to balance the effects of these two types of loss terms. We set it to 0.01, following Zhou et al. [2023], and found that this configuration is sufficient to produce graphs that closely resemble the reference graphs without further tuning. To better elucidate the optimization objective, we list out the following analytical expressions:

$$\begin{aligned}
& \text{KL}(p_\theta(\mathbf{G}_{t-1} | \mathbf{G}_t) \| q(\mathbf{G}_{t-1} | \mathbf{G}_t, \mathbf{G}_0)) \\
&= \ln \Gamma(\eta(\alpha_{t-1} - \alpha_t)\mathbf{G}_0) + \ln \Gamma(\eta - \eta\alpha_{t-1}\mathbf{G}_0) + \ln \Gamma(\eta - \eta\alpha_t\mathbf{G}_0) \\
&\quad - \ln \Gamma(\eta(\alpha_{t-1} - \alpha_t)\hat{\mathbf{G}}_0) - \ln \Gamma(\eta - \eta\alpha_{t-1}\hat{\mathbf{G}}_0) - \ln \Gamma(\eta - \eta\alpha_t\hat{\mathbf{G}}_0) \\
&\quad + \eta(\alpha_{t-1} - \alpha_t)(\hat{\mathbf{G}}_0 - \mathbf{G}_0) \cdot \psi(\eta(\alpha_{t-1} - \alpha_t)\hat{\mathbf{G}}_0) \\
&\quad + \eta\alpha_{t-1}(\mathbf{G}_0 - \hat{\mathbf{G}}_0) \cdot \psi(\eta - \eta\alpha_{t-1}\hat{\mathbf{G}}_0) \\
&\quad + \eta\alpha_t(\mathbf{G}_0 - \hat{\mathbf{G}}_0) \cdot \psi(\eta - \eta\alpha_t\hat{\mathbf{G}}_0),
\end{aligned} \tag{11}$$

$$\begin{aligned}
& \text{KL}\left(q(\mathbf{G}_\tau | \hat{G}_\theta(\mathbf{G}_t, t)) \| q(\mathbf{G}_\tau | \mathbf{G}_0)\right) \\
&= \ln \Gamma(\eta\alpha_t\mathbf{G}_0) + \ln \Gamma(\eta - \eta\alpha_t\mathbf{G}_0) - \ln \Gamma(\eta\alpha_t\hat{\mathbf{G}}_0) - \ln \Gamma(\eta - \eta\alpha_t\hat{\mathbf{G}}_0) \\
&\quad + \eta\alpha_t(\hat{\mathbf{G}}_0 - \mathbf{G}_0) \cdot \left(\psi(\eta\alpha_t\hat{\mathbf{G}}_0) - \psi(\eta - \eta\alpha_t\hat{\mathbf{G}}_0)\right),
\end{aligned} \tag{12}$$

where $\hat{\mathbf{G}}_0 := \hat{G}_\theta(\mathbf{G}_t, t)$.

It is demonstrated in Zhou et al. [2023] that the KL divergence between two beta distributions can be expressed in the format of a Bregman divergence. Namely, considering a convex function $\phi(\alpha, \beta) \triangleq \ln \text{Beta}(\alpha, \beta)$, where $\text{Beta}(\alpha, \beta) = \frac{\Gamma(\alpha)\Gamma(\beta)}{\Gamma(\alpha+\beta)}$ is the beta function, the loss term $\mathcal{L}_{\text{sampling}}$ can be expressed as

$$\begin{aligned}
\mathcal{L}_{\text{sampling}}(t, \mathbf{G}_0) &= \mathbb{E}_{q(\mathbf{G}_t)} \mathbb{E}_{q(\mathbf{G}_0 | \mathbf{G}_t)} d_\phi\left([\mathbf{a}_{\text{sampling}}, \mathbf{b}_{\text{sampling}}], [\mathbf{a}_{\text{sampling}}^*, \mathbf{b}_{\text{sampling}}^*]\right), \\
\mathbf{a}_{\text{sampling}} &= \eta(\alpha_{t-1} - \alpha_t)\mathbf{G}_0, \quad \mathbf{b}_{\text{sampling}} = \eta(1 - \alpha_{t-1}\mathbf{G}_0), \\
\mathbf{a}_{\text{sampling}}^* &= \eta(\alpha_{t-1} - \alpha_t)\hat{\mathbf{G}}_0, \quad \mathbf{b}_{\text{sampling}}^* = \eta(1 - \alpha_{t-1}\hat{\mathbf{G}}_0).
\end{aligned} \tag{13}$$

Likewise, we can express the correction loss term $\mathcal{L}_{\text{correction}}$ as

$$\begin{aligned}
\mathcal{L}_{\text{correction}}(t, \mathbf{G}_0) &= \mathbb{E}_{q(\mathbf{G}_t)} \mathbb{E}_{q(\mathbf{G}_0 | \mathbf{G}_t)} d_\phi\left([\mathbf{a}_{\text{correction}}, \mathbf{b}_{\text{correction}}], [\mathbf{a}_{\text{correction}}^*, \mathbf{b}_{\text{correction}}^*]\right), \\
\mathbf{a}_{\text{correction}} &= \eta\alpha_t\mathbf{G}_0, \quad \mathbf{b}_{\text{correction}} = \eta(1 - \alpha_t\mathbf{G}_0), \\
\mathbf{a}_{\text{correction}}^* &= \eta\alpha_t\hat{\mathbf{G}}_0, \quad \mathbf{b}_{\text{correction}}^* = \eta(1 - \alpha_t\hat{\mathbf{G}}_0).
\end{aligned} \tag{14}$$

Here we reference the d_ϕ notation of Banerjee et al. [2005] to represent the Bregman divergence. As stated in Lemmas 3-5 of Zhou et al. [2023], one can apply Proposition 1 of Banerjee et al. [2005] to show that both $\mathcal{L}_{\text{sampling}}$ and $\mathcal{L}_{\text{correction}}$ yield the same optimal solution that legitimates the usage of $\hat{\mathbf{G}}_0$ in the reverse diffusion process.

Property 1. *Both $\mathcal{L}_{\text{sampling}}$ and $\mathcal{L}_{\text{correction}}$ are uniquely minimized at*

$$\hat{\mathbf{G}}_0 = \hat{G}_\theta(\mathbf{G}_t, t) = \mathbb{E}_{q(\mathbf{G}_0 | \mathbf{G}_t)}[\mathbf{G}_0].$$

Algorithm 3 Training, in original domain.

Require: Number of timesteps $T = 1000$, default concentration parameter $\eta = 30$, predictor \hat{G}_θ , default node influence factor $\gamma = 0.5$, input graph batch $\mathbb{B} = \{\mathbf{G}^{(k)} = (\mathbf{A}^{(k)}, \mathbf{X}^{(k)})\}_{[K]}$, default learning rate $\lambda = 0.002$, optimization steps M .

- 1: (Optional) Assign value to η via Equation (16)
- 2: **for** step = 1 to M **do**
- 3: Initialize \mathcal{L}_X and \mathcal{L}_A with 0
- 4: **for** $k = 1$ to K **do**
- 5: $t \sim \text{Unif}(1, \dots, T)$
- 6: $\alpha_t, \alpha_{t-1} \leftarrow \text{schedule}(t), \text{schedule}(t-1)$
- 7: $\mathbf{A}_0 \leftarrow w_A \cdot \mathbf{A}^{(k)} + b_A$
- 8: $\mathbf{X}_0 \leftarrow w_X \cdot \mathbf{X}^{(k)} + b_X$
- 9: $\mathbf{G}_0 \leftarrow (\mathbf{A}_0, \mathbf{X}_0)$
- 10: $\mathbf{G}_t \sim \text{Beta}(\eta\alpha_t \mathbf{G}_0, \eta(1 - \alpha_t \mathbf{G}_0))$
- 11: $\mathbf{G}_{in} \leftarrow \frac{\mathbf{G}_t - \mathbb{E}[\mathbf{G}_t]}{\sqrt{\text{Var}[\mathbf{G}_t]}}$
- 12: $(\hat{\mathbf{A}}'_0, \hat{\mathbf{X}}'_0) \leftarrow \hat{\mathbf{G}}_\theta(\mathbf{G}_{in}, t)$
- 13: $\hat{\mathbf{A}}_0 = w_A \cdot \hat{\mathbf{A}}'_0 + b_A$
- 14: $\hat{\mathbf{X}}_0 = w_X \cdot \hat{\mathbf{X}}'_0 + b_X$
- 15: $\mathcal{L}_A \leftarrow \mathcal{L}_A + \mathcal{L}(\mathbf{A}_0, \hat{\mathbf{A}}_0, \eta, \alpha_t, \alpha_{t-1})$
- 16: $\mathcal{L}_X \leftarrow \mathcal{L}_X + \mathcal{L}(\mathbf{X}_0, \hat{\mathbf{X}}_0, \eta, \alpha_t, \alpha_{t-1})$
- 17: **end for**
- 18: $\theta \leftarrow \theta - \frac{\lambda}{K} \nabla_\theta(\mathcal{L}_A + \gamma \mathcal{L}_X)$
- 19: **end for**

Algorithm 4 Training, in logit domain.

Require: Number of timesteps T , concentration parameter η , predictor \hat{G}_θ , node influence factor γ , input graph batch \mathbb{B} , learning rate λ , optimization steps M . Same default values with Algorithm 3.

- 1: **for** step = 1 to M **do**
- 2: Initialize \mathcal{L}_X and \mathcal{L}_A with 0
- 3: **for** $k = 1$ to K **do**
- 4: $t \sim \text{Unif}(1, \dots, T)$
- 5: $\alpha_t, \alpha_{t-1} \leftarrow \text{schedule}(t), \text{schedule}(t-1)$
- 6: $\mathbf{A}_0 \leftarrow w_A \cdot \mathbf{A}^{(k)} + b_A$
- 7: $\mathbf{X}_0 \leftarrow w_X \cdot \mathbf{X}^{(k)} + b_X$
- 8: $\mathbf{G}_0 \leftarrow (\mathbf{A}_0, \mathbf{X}_0)$
- 9: $\mathbf{U}_t \sim \text{Gamma}(\eta\alpha_t \mathbf{G}_0, 1)$
- 10: $\mathbf{V}_t \sim \text{Gamma}(\eta(1 - \alpha_t \mathbf{G}_0), 1)$
- 11: $\text{logit}(\mathbf{G}_t) \leftarrow \ln \mathbf{U}_t - \ln \mathbf{V}_t$
- 12: $\mathbf{G}_{in} \leftarrow \frac{\text{logit}(\mathbf{G}_t) - \mathbb{E}[\text{logit}(\mathbf{G}_t)]}{\sqrt{\text{Var}[\text{logit}(\mathbf{G}_t)]}}$
- 13: $(\hat{\mathbf{A}}'_0, \hat{\mathbf{X}}'_0) \leftarrow \hat{\mathbf{G}}_\theta(\mathbf{G}_{in}, t)$
- 14: $\hat{\mathbf{A}}_0 = w_A \cdot \hat{\mathbf{A}}'_0 + b_A$
- 15: $\hat{\mathbf{X}}_0 = w_X \cdot \hat{\mathbf{X}}'_0 + b_X$
- 16: $\mathcal{L}_A \leftarrow \mathcal{L}_A + \mathcal{L}(\mathbf{A}_0, \hat{\mathbf{A}}_0, \eta, \alpha_t, \alpha_{t-1})$
- 17: $\mathcal{L}_X \leftarrow \mathcal{L}_X + \mathcal{L}(\mathbf{X}_0, \hat{\mathbf{X}}_0, \eta, \alpha_t, \alpha_{t-1})$
- 18: **end for**
- 19: $\theta \leftarrow \theta - \frac{\lambda}{K} \nabla_\theta(\mathcal{L}_A + \gamma \mathcal{L}_X)$
- 20: **end for**

2.4 Exploring the design space of GBD

Many diffusion-based graph generative models offer great flexibility with technical adjustment to enhance their practical performances. Here we list four impactful dimensions among the design space of GBD. Namely, data transformation, concentration modulation, logit-domain computation, and neural-network precondition. We elaborate each design dimension below and discuss our choices in these aspects in the appendix.

Data transformation. We convert the raw data (\mathbf{A}, \mathbf{X}) to \mathbf{G}_0 through linear transformations, *i.e.*,

$$\mathbf{G}_0 = (\mathbf{A}_0, \mathbf{X}_0), \text{ where } \mathbf{A}_0 = w_A \cdot \mathbf{A} + b_A, \mathbf{X}_0 = w_X \cdot \mathbf{X} + b_X, \quad (15)$$

with the constraints that $\min(w_A, b_A, w_X, b_X) > 0$ and $\max(w_A + b_A, w_X + b_X) \leq 1$. This operation not only ensure that all data values fall within the positive support of beta distributions, avoiding gradient explosion when optimizing the loss function, but also provide an effective means to adjust the rate at which diffusion trajectories mix. A forward diffusion trajectory reaches a state of “mix” when it becomes indistinguishable to discern the initial value from its counterfactual given the current value. A suitable mixing rate ensures that the signal-to-noise ratio (SNR) of the final state in the forward diffusion process approaches zero, meeting the prerequisite for learning reverse diffusion while preserving the learnability of graph structural patterns. The scaling parameter provides a macro control for the mixing rate, with a smaller value contracting the data range and promoting the arrival of the mixing state.

Concentration modulation. Another hyperparameter that offers a more refined adjustment to the mixing rate is the concentration parameter η . Higher values of η reduce the variance of the fractional multipliers \mathbf{P}_t sampled from their corresponding beta distributions, thus delaying the arrival of the mixing state. Leveraging

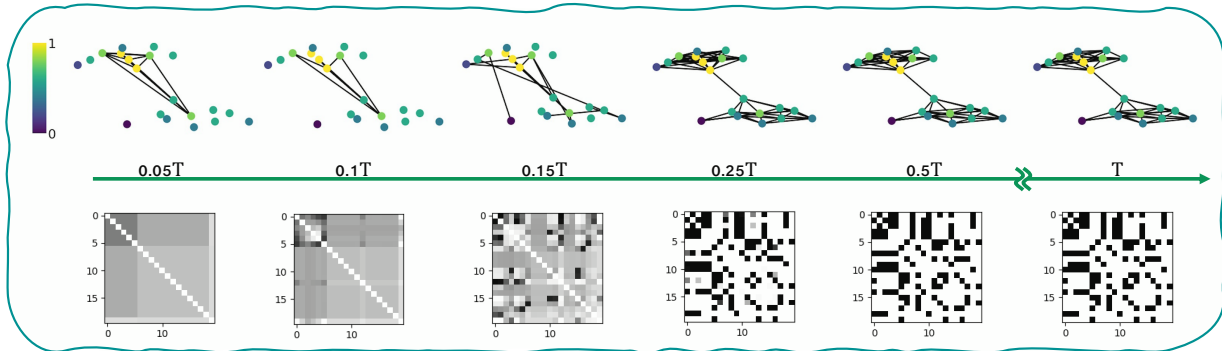


Figure 2: Reverse Process on Graph Edges: Each edge (u, v) undergoes a reverse process with specific $\eta_{u,v}$ parameters, influenced by $\deg(u)$ and $\deg(v)$. The colorbar indicates the normalized degree of nodes in the final graph, with brighter colors (shifting towards yellow) denoting higher degrees. Nodes in the adjacency matrices shown in the bottom row are reordered based on decreasing node degree.

this property, we have devised a simple yet effective modulation strategy to differentiate the mixing time for various graph substructures.

Specifically, we assign higher η values to “important positions” within a graph, such as edges connecting high-degree nodes or edges redeemed as significant based on domain knowledge, such as the carbon-carbon bond in chemical molecules. For instance, when modulating η from node degrees, the exact operation executed upon the η values for edge (u, v) and for the features of node u can be mathematically expressed as

$$\eta_{u,v} = g_A(\max(\deg(u), \deg(v))), \quad \eta_u = g_X(\deg(u)). \quad (16)$$

Here we first prepare several levels of η values, then utilize two assignment functions, namely $g_A(\cdot)$ and $g_X(\cdot)$, to map the node degrees (or their percentile in the degree population) to one of the choices of the η values. We have observed that this operation indeed prolongs the presence of these substructures during the forward diffusion process, which in turn leads to their earlier emergence compared to the rest of the graph during the reverse process.

We visualize the reverse process from two perspectives in Figure 2. We first obtain the $\eta_{u,v}$ by degrees retrieved from the training set before sampling and then generate graph through reverse beta diffusion. From the top row, we observe that edges linked to nodes with higher degrees (indicated by brighter colors) appear first, followed by other edges. From the bottom row, it is evident that edges connected to the first five nodes, which have higher degrees, are identified first and then progressively in descending order of degree. Notably, the nodes of the adjacency matrices in the bottom row are reordered by decreasing node degree of the final graph. Additionally, we can also find the predicted graph of GBD converges in an early stage to the correct topology. We attribute the enhanced quality of generated graphs to the early emergence of these “important substructures,” which potentially enhances the reliability of generating realistic graph structures. Furthermore, we find this approach particularly appealing because it allows for the flexible integration of graph inductive biases within the diffusion model framework.

Logit domain computation. Another noteworthy designing direction lies in the computation domain. Although the reverse sampling process directly implemented from Equation (5) is already effective to generate realistic graph data, we observe that migrating the computation to the logit space further enhances model performance and accelerates training convergence. One potential explanation is that the logit transformation amplifies the structural patterns of the graph when all edge weights are very close to zero at the beginning of the ancestral sampling process. Equivalent to Equation (5), the logit-domain computation can be expressed as

$$\text{logit}(\mathbf{G}_{t-1}) = \ln \left(e^{\text{logit}(\mathbf{G}_t)} + e^{\text{logit}(\mathbf{P}_t)} + e^{\text{logit}(\mathbf{G}_t) + \text{logit}(\mathbf{P}_t)} \right). \quad (17)$$

Neural-network precondition. A drawback of the logit-domain computation is its introduction of variability to model training, we address this issue by employing neural-network precondition techniques [Karras et al., 2022]. Specifically, precondition involves standardizing \mathbf{G}_t before passing them to the prediction network $\hat{G}_\theta(\cdot)$. In other words, we modify Equation (7) as

$$p_\theta(\mathbf{G}_{t-1} \mid \mathbf{G}_t) := q(\mathbf{G}_{t-1} \mid \mathbf{G}_t, \hat{G}_\theta(\tilde{\mathbf{G}}_t, t)), \quad \tilde{\mathbf{G}}_t = \frac{\mathbf{G}_t - \mathbb{E}[g_t]}{\sqrt{\text{Var}[g_t]}} \text{ or } \frac{\text{logit}(\mathbf{G}_t) - \mathbb{E}[\text{logit}(g_t)]}{\sqrt{\text{Var}[\text{logit}(g_t)]}}, \quad (18)$$

where g_t denotes the elements within \mathbf{G}_t . Based upon the law of total expectation and the law of total variance, Zhou et al. [2023] have derived the following attribute of beta diffusion

Attribute 1. *Given that $g_t|g_0 \sim \text{Beta}(\eta\alpha_t g_0, \eta(1-\alpha_t g_0))$, one can derive that $\mathbb{E}[g_t|g_0] = \alpha_t g_0$ and $\text{Var}[g_t|g_0] = \frac{\alpha_t g_0(1-\alpha_t g_0)}{\eta+1}$. Representing $\mathbb{E}[g_0]$ and $\text{Var}[g_0]$ with μ and σ^2 , we have*

$$\mathbb{E}[g_t] = \alpha_t \mu, \quad \text{Var}[g_t] = \frac{\alpha_t \mu - \alpha_t^2(\mu^2 + \sigma^2)}{\eta + 1} + \alpha_t^2 \sigma^2.$$

Their counterparts in the logit domain are expressed as

$$\begin{aligned} \mathbb{E}[\text{logit}(g_t)] &= \mathbb{E}[\psi(\eta\alpha_t g_0)] - \mathbb{E}[\psi(\eta - \eta\alpha_t g_0)], \\ \text{Var}[\text{logit}(g_t)] &= \mathbb{E}[\psi^{(1)}(\eta\alpha_t g_0)] + \mathbb{E}[\psi^{(1)}(\eta(1 - \alpha_t g_0))] + \text{Var}[\psi(\eta\alpha_t g_0)] + \text{Var}[\psi(\eta(1 - \alpha_t g_0))], \end{aligned}$$

with $\psi(\cdot)$ and $\psi^{(1)}(\cdot)$ denoting digamma and trigamma functions.

In addition to Attribute 1, the specific values for $\mathbb{E}[g_t]$, $\text{Var}[g_t]$, $\mathbb{E}[\text{logit}(g_t)]$ and $\text{Var}[\text{logit}(g_t)]$ are also reliant on the distribution of the datum in its initial state. Recall that all variables within \mathbf{G}_0 have been preprocessed using either dummy encoding or CDF transformation. Consequently, the processed variables follow either a discrete distribution or a uniform distribution. With this context, if the original datum follows a discrete distribution, we present the following conclusion.

Remark 1. *If g_0 has two potential outcomes $\{g_{\min}, g_{\max}\}$ with $P(g_0 = g_{\max}) = p$, then*

$$\begin{aligned} \mathbb{E}[g_t] &= \alpha_t (p \cdot g_{\max} + (1-p) \cdot g_{\min}), \\ \text{Var}[g_t] &= \frac{1}{\eta+1} (\mathbb{E}[g_t] - \mathbb{E}[g_t]^2) + \frac{\eta}{\eta+1} (\alpha_t^2 (p(1-p))(g_{\max} - g_{\min})^2). \end{aligned} \quad (19)$$

The calculation of $\mathbb{E}[\text{logit}(g_t)]$ and $\text{Var}[\text{logit}(g_t)]$ relies on a series of components, namely

$$\begin{aligned} \mathbb{E}[\psi(\eta\alpha_t g_0)] &= p \cdot \psi(\eta\alpha_t g_{\max}) + (1-p) \cdot \psi(\eta\alpha_t g_{\min}), \\ \mathbb{E}[\psi(\eta - \eta\alpha_t g_0)] &= p \cdot \psi(\eta - \eta\alpha_t g_{\max}) + (1-p) \cdot \psi(\eta - \eta\alpha_t g_{\min}), \\ \text{Var}[\psi(\eta\alpha_t g_0)] &= p(1-p) (\psi(\eta\alpha_t g_{\max}) - \psi(\eta\alpha_t g_{\min}))^2, \\ \text{Var}[\psi(\eta - \eta\alpha_t g_0)] &= p(1-p) (\psi(\eta - \eta\alpha_t g_{\max}) - \psi(\eta - \eta\alpha_t g_{\min}))^2, \\ \mathbb{E}[\psi^{(1)}(\eta\alpha_t g_0)] &= p \cdot \psi^{(1)}(\eta\alpha_t g_{\max}) + (1-p) \cdot \psi^{(1)}(\eta\alpha_t g_{\min}), \\ \mathbb{E}[\psi^{(1)}(\eta - \eta\alpha_t g_0)] &= p \cdot \psi^{(1)}(\eta - \eta\alpha_t g_{\max}) + (1-p) \cdot \psi^{(1)}(\eta - \eta\alpha_t g_{\min}), \end{aligned} \quad (20)$$

with which one can easily deduce the expressions of $\mathbb{E}[\text{logit}(g_t)]$ and $\text{Var}[\text{logit}(g_t)]$ following Attribute 1.

Alternatively, if the original datum follows a uniform distribution upon the support $[g_{\min}, g_{\max}]$, then as demonstrated in Zhou et al. [2023], we have

Remark 2. *If g_0 follows the uniform distribution $\text{Unif}[g_{\min}, g_{\max}]$, then*

$$\begin{aligned} \mathbb{E}[g_t] &= \frac{1}{2} \alpha_t (g_{\min} + g_{\max}), \\ \text{Var}[g_t] &= \frac{1}{\eta+1} (\mathbb{E}[g_t] - \mathbb{E}[g_t]^2) + \frac{\eta}{12(\eta+1)} (\alpha_t^2 (g_{\max} - g_{\min})^2). \end{aligned} \quad (21)$$

We denote by K the number of sub-intervals used in the numerical integration based on the Trapezoidal rule. Similar to Remark 1, on the logit domain, we list out the expressions for the components as

$$\begin{aligned}
\mathbb{E}[\psi(\eta\alpha_t g_0)] &= \frac{1}{\eta\alpha_t(g_{\max} - g_{\min})} (\ln \Gamma(\eta\alpha_t g_{\max}) - \ln \Gamma(\eta\alpha_t g_{\min})), \\
\mathbb{E}[\psi(\eta - \eta\alpha_t g_0)] &= \frac{1}{\eta\alpha_t(g_{\max} - g_{\min})} (\ln \Gamma(\eta - \eta\alpha_t g_{\min}) - \ln \Gamma(\eta - \eta\alpha_t g_{\max})), \\
\text{Var}[\psi(\eta\alpha_t g_0)] &\approx \max \left(\frac{1}{K} \sum_{i=0}^K \frac{\psi^2 \left(\eta\alpha_t \left(g_{\min} + \frac{i}{K}(g_{\max} - g_{\min}) \right) \right)}{2^{\delta(i=0)+\delta(i=K)}} - \mathbb{E}[\psi(\eta\alpha_t g_0)]^2, 0 \right), \\
\text{Var}[\psi(\eta - \eta\alpha_t g_0)] &\approx \max \left(\frac{1}{K} \sum_{i=0}^K \frac{\psi^2 \left(\eta - \eta\alpha_t \left(g_{\min} + \frac{i}{K}(g_{\max} - g_{\min}) \right) \right)}{2^{\delta(i=0)+\delta(i=K)}} - \mathbb{E}[\psi(\eta - \eta\alpha_t g_0)]^2, 0 \right), \\
\mathbb{E}[\psi^{(1)}(\eta\alpha_t g_0)] &= \frac{1}{\eta\alpha_t(g_{\max} - g_{\min})} (\psi(\eta\alpha_t g_{\max}) - \psi(\eta\alpha_t g_{\min})), \\
\mathbb{E}[\psi^{(1)}(\eta - \eta\alpha_t g_0)] &= \frac{1}{\eta\alpha_t(g_{\max} - g_{\min})} (\psi(\eta - \eta\alpha_t g_{\min}) - \psi(\eta - \eta\alpha_t g_{\max})). \tag{22}
\end{aligned}$$

Utilizing Attribute 1, one can derive the mathematical expressions that we use to calculate $\mathbb{E}[\text{logit}(g_t)]$ and $\text{Var}[\text{logit}(g_t)]$.

3 Related Work

Graph generative models. Early attempts at modeling graph distributions trace back to the Erdős–Rényi random graph model [ERDdS and R&wi, 1959, Erdős et al., 1960], from which a plethora of graph generative models have emerged. These models employ diverse approaches to establish the data generative process and devise optimization objectives, which in turn have significantly expanded the flexibility in modeling the distribution of graph data. Stochastic blockmodels [Holland et al., 1983, Lee and Wilkinson, 2019], more advanced latent variable models [Airoldi et al., 2009, Zhou, 2015, Caron and Fox, 2017], and their variational-autoencoder-based successors [Kipf and Welling, 2016, Hasanzadeh et al., 2019, Mehta et al., 2019, He et al., 2022] assume that edges are formed through independent pairwise node interactions, and thus factorize the probability of the graph adjacency matrix into the dot product of factor representations of nodes. Sequential models [You et al., 2018, Wang et al., 2018, Jin et al., 2018, Han et al., 2023] adopt a similar concept of node interactions but correlate these interactions by organizing them into a series of connection events. Additionally, some models treat the graph adjacency matrix as a parameterized random matrix and generate it by mapping a random vector through a feed-forward neural network [Simonovsky and Komodakis, 2018, De Cao and Kipf, 2018]. In terms of optimization targets, many utilize log-likelihood-based objectives such as negative log-likelihood [Liu et al., 2019] or evidence lower bound objectives [Kipf and Welling, 2016], while others employ generative adversarial losses [Wang et al., 2018] or reinforcement learning losses [De Cao and Kipf, 2018]. Diffusion-based graph generative models [Jo et al., 2022, Haefeli et al., 2022, Vignac et al., 2023, Jo et al., 2023, Chen et al., 2023, Cho et al., 2023, Kong et al., 2023], including this work, feature a unique data generation process compared to previous models. They map the observed graph structures and node features to a latent space through a stochastic diffusion process, whose reverse process can be learned by optimizing a variational lower bound [Vignac et al., 2023] or numerically solving a reverse stochastic differential equation [Jo et al., 2022].

Diffusion models. The stochastic diffusion process is introduced by Sohl-Dickstein et al. [2015] for deep unsupervised learning, and its foundational connection with deep generative models is laid down by denoising diffusion probabilistic model (DDPM) [Ho et al., 2020]. DDPM maps a data sample to the latent space via a Markov process that gradually applies noise to the original sample, and learns a reverse process to reproduce the sample in finite steps. The optimization and sampling processes in DDPM can be interpreted through the lens of variational inference [Sohl-Dickstein et al., 2015, Ho et al., 2020] or can be formulated as score

matching with Langevin dynamics [Song et al., 2021, Song and Ermon, 2019]. Both approaches are focused on diffusion processes that define the transition between normally distributed variables, which are proven effective for generating natural images. As the scope of generative tasks expands to discrete domains like text, diffusion models transitioning between discrete states emerge [Austin et al., 2021], which demonstrates that the choice of probabilistic distribution for modeling each noise state could significantly impact the learning task. This conclusion is also validated in the application of graph generation [Haefeli et al., 2022, Vignac et al., 2023]. Further studies [Chen and Zhou, 2023, Zhou et al., 2023] are conducted to improve diffusion models by introducing novel diffusion processes based on probabilistic distributions that better capture the intrinsic characteristics of the generation target. Among these, the beta diffusion of Zhou et al. [2023] is chosen as the foundation of our method, due to the beta distribution’s proficiency in capturing sparsity and long-tailed characteristics in range-bounded data. These traits are commonly observed in real-world graphs [Barabási et al., 2000, Ciotti et al., 2015, Liang et al., 2023, Wang et al., 2023].

4 Experiments

We validated GBD on both molecular and non-molecular benchmarks, demonstrating its ability to generate valid graphs using various evaluation metrics.

4.1 Generic graph generation

To verify that GBD can generate graphs accurately reflecting the underlying data distribution, we first evaluate our method on a range of generic generation tasks across various datasets.

Datasets and metrics. We consider three synthetic and real datasets of varying size and connectivity used as benchmarks in previous works: **Ego-small** consists of 200 small real sub-graphs from the Citeseer network dataset with $4 \leq N \leq 18$, where N denotes the number of nodes. **Community-small** consists of 100 randomly generated synthetic graphs with $12 \leq N \leq 20$. **Grid** consists of randomly generated 100 standard 2D grid graphs with $100 \leq N \leq 400$.

For a fair comparison, we follow the experimental and evaluation setting of Jo et al. [2022, 2023] with the same train/test split. We adopt maximum mean discrepancy (MMD) [Gretton et al., 2012] as our evaluation metric to compare three graph property distributions between the test graphs and the same number of generated graphs: degree (**Deg.**), clustering coefficient (**Clus.**), count of orbits with 4 nodes (**Orbit**), and their average score (**Avg.**). Further details about these metrics can be found in Appendix A.

Baselines. We compare GBD against the following autoregressive and one-shot graph generation methods: **DeepGMG** [Li et al., 2018], **GraphRNN** [You et al., 2018], **GraphAF** [Shi et al., 2020], **GraphDF** [Luo et al., 2021], **GraphVAE** [Simonovsky and Komodakis, 2018], and **GNF** [Liu et al., 2019]. We also compare GBD against several state-of-the-art diffusion-based graph generative models: **EDP-GNN** [Niu et al., 2020a], a score-based model for adjacency matrix, **GDSS** [Jo et al., 2022] and **ConGress** [Vignac et al., 2023], continuous diffusion models, **DiGress** [Vignac et al., 2023], a discrete diffusion model, and **Wave-GD** [Cho et al., 2023], a wavelet-based diffusion model. We describe implementation details in Appendix A.

Results. As shown in Table 1, the proposed GBD achieves superior or comparable performance to the MMD of the sampled graphs from the training set. Compared to previous diffusion-based methods, GBD outperforms them on 7/9 MMD metrics and achieves the best average results on each dataset. In particular, GBD surpasses DiGress on all MMD metrics, demonstrating that our model is capable of modeling discrete graph data and even achieves better results. We attribute this to our model’s superior ability to capture the sparsity of the graph data distribution, which makes GBD distinctive. For the larger graph dataset Grid,

Table 1: Generic graph generation results.

Method	Ego-small				Community-small				Grid			
	Deg. ↓	Clus. ↓	Orbit. ↓	Avg. ↓	Deg. ↓	Clus. ↓	Orbit. ↓	Avg. ↓	Deg. ↓	Clus. ↓	Orbit. ↓	Avg. ↓
DeepGMG	0.040	0.100	0.020	0.053	0.220	0.950	0.400	0.523	-	-	-	-
GraphRNN	0.090	0.220	0.003	0.104	0.080	0.120	0.040	0.080	0.064	0.043	0.021	0.043
GraphAF	0.030	0.110	0.001	0.047	0.180	0.200	0.020	0.133	-	-	-	-
GraphDF	0.040	0.130	0.010	0.060	0.060	0.120	0.030	0.070	-	-	-	-
GraphVAE	0.130	0.170	0.050	0.117	0.350	0.980	0.540	0.623	1.619	0.0	0.919	0.846
GNF	0.030	0.100	0.001	0.044	0.200	0.200	0.110	0.170	-	-	-	-
EDP-GNN	0.052	0.093	0.007	0.051	0.053	0.144	0.026	0.074	0.455	0.238	0.328	0.340
GDSS	0.021	0.024	0.007	0.017	0.045	0.086	0.007	0.046	0.111	0.005	0.070	0.062
ConGress*	0.037	0.064	0.017	0.039	0.020	0.076	0.006	0.034	-	-	-	-
DiGress	0.017	0.021	0.010	0.016	0.028	0.115	0.009	0.050	-	-	-	-
Wave-GD	0.012	0.010	0.005	0.009	0.007	0.058	0.002	0.022	0.144	0.004	0.021	0.056
GBD	0.011	0.014	0.002	0.009	0.002	0.060	0.002	0.021	0.045	0.011	0.040	0.032
	(±0.008)	(±0.013)	(±0.004)	-	(±0.003)	(±0.004)	(±0.003)	-	(±0.004)	(±0.002)	(±0.014)	-

GBD obtains a superior average score and other competitive MMDs compared to Wave-GD, demonstrating its potential in generating larger graphs.

Evaluation with larger sample size. For Ego-small and Community-small, it is worth noting that for most evaluation metrics, the MMDs of the graphs sampled from the training set still have large standard deviations, likely due to the small number of nodes in the graph and the insufficient size of the sampled graphs. Therefore, it is necessary to assess the quality of generated samples more definitively using a larger number of generated graphs compared to the test data. Similar to the previous works [Cho et al., 2023, Jo et al., 2022, Liu et al., 2019], we sampled 1024 graphs for each smaller dataset and evaluated the MMD metrics with their means and standard deviations reported in Table 2. We observe that our proposed GBD outperforms previous continuous and discrete diffusion models on both smaller datasets. Furthermore, GBD significantly surpasses the wavelet-based diffusion model (Wave-GD) by a wide margin on the Community-small dataset, as evidenced by both means and standard deviations. Specifically, GBD achieves 85.0%, 90.5%, and 40.0% improvements over Wave-GD in the MMDs means of Degree, Cluster, and Orbit, respectively, indicating that our model is capable of generating smaller graphs that are closer to the data distribution with better stability.

Table 2: Generic graph generation results with larger sample size.

Method	Ego-small				Community-small			
	Deg. ↓	Clus. ↓	Orbit. ↓	Avg. ↓	Deg. ↓	Clus. ↓	Orbit. ↓	Avg. ↓
GraphRNN	0.040	0.050	0.060	0.050	0.030	0.010	0.010	0.017
GNF	0.010	0.030	0.001	0.014	0.120	0.150	0.020	0.097
EDP-GNN	0.010	0.025	0.003	0.013	0.006	0.127	0.018	0.050
GDSS	0.023	0.020	0.005	0.016	0.029	0.068	0.004	0.034
ConGress*	0.030	0.050	0.008	0.030	0.004	0.047	0.001	0.017
	(± 0.001)	(± 0.003)	(± 0.001)	-	(± 0.000)	(± 0.000)	(± 0.000)	-
DiGress*	0.009	0.031	0.003	0.014	0.003	0.009	0.001	0.004
	(± 0.000)	(± 0.002)	(± 0.000)	-	(± 0.000)	(± 0.001)	(± 0.000)	-
Wave-GD	0.010	0.018	0.005	0.011	0.016	0.077	0.001	0.031
	(± 0.001)	(± 0.003)	(± 0.002)	-	(± 0.000)	(± 0.006)	(± 0.002)	-
GBD	0.007	0.011	0.003	0.010	0.002	0.007	0.001	0.003
	(± 0.000)	(± 0.001)	(± 0.000)	-	(± 0.000)	(± 0.001)	(± 0.000)	-

Table 3: 2D molecule generation results

Method	QM9 ($ V \leq 9$)				ZINC250K			
	Valid (%) \uparrow	FCD \downarrow	NSPDK \downarrow	Scaf. \downarrow	Valid(%) \uparrow	FCD \downarrow	NSPDK \downarrow	Scaf. \downarrow
MoFlow	91.36	4.467	0.0169	0.1447	63.11	20.931	0.0455	0.0133
GraphAF	74.43	5.625	0.0207	0.3046	68.47	16.023	0.0442	0.0672
GraphDF	93.88	10.928	0.0636	0.0978	90.61	33.546	0.1770	0.0000
EDP-GNN	47.52	2.680	0.0046	0.3270	82.97	16.737	0.0485	
GDSS	95.72	2.900	0.0033	0.6983	97.01	14.656	0.0195	0.0467
GDSS+Transformer	99.68	0.737	0.0024	0.9129	96.04	5.556	0.0326	0.3205
DiGress	98.19	0.095	0.0003	0.9353	94.99	3.482	0.0021	0.4163
DruM	99.69	0.108	0.0002	0.9449	98.65	2.257	0.0015	0.5299
GBD	99.88	0.093	0.0002	0.9510	97.87	2.248	0.0018	0.5042

4.2 Molecule Generation

We validate GBD on 2D molecule generation tasks for attributed graphs, demonstrating its capability to model graph structure with both node and edge attributes.

Datasets and Metrics We consider two widely-used molecule datasets as benchmarks in Jo et al. [2022]: QM9 [Ramakrishnan et al., 2014], which consists of 133,885 molecules with $N \leq 9$ nodes from 4 different node types, and ZINC250k [Irwin et al., 2012], which consists of 249,455 molecules with $N \leq 38$ nodes from 9 different node types. Molecules in both datasets have 3 edge types, namely single bond, double bond, and triple bond.

Following the evaluation setting of Jo et al. [2022], we generated 10,000 molecules for each dataset and evaluate them with four metrics: the ratio of valid molecules without correction (**Val.**), Fréchet ChemNet Distance (**FCD**), Neighborhood subgraph pairwise distance kernel **NSPDK**, and Scaffold similarity (**Scaf.**).

Baselines We compare GBD against the following autoregressive and one-shot graph generation methods: **MoFlow** [Zang and Wang, 2020], **GraphAF** [Shi et al., 2020], **GraphDF** [Luo et al., 2021], and several state-of-the-art diffusion-based graph generative models discussed previously: **EDP-GNN** [Niu et al., 2020a], **GDSS** [Jo et al., 2022] and **ConGress** [Vignac et al., 2023], **DiGress** [Vignac et al., 2023], and **DruM** [Jo et al., 2023]. We describe the implementation details in Appendix A.

Results As shown in Table 3, we observe that our GBD outperforms most previous diffusion-based models and is competitive with the current state-of-the-art Gaussian-based diffusion model, DruM. In particular, compared to the basic continuous diffusion model, GBD significantly outperforms it (GDSS+Transformer) under the same GraphTransformer architecture. Additionally, we observe that our proposed beta-based diffusion model is superior to the discrete diffusion model on both 2D molecule datasets, demonstrating that the beta-based diffusion model is also capable of modeling complex structures of attributed graphs (even more effectively when comparing GBD to DiGress). We attribute this to the excellent modeling ability of beta-based diffusion model for sparse and long-tailed data distributions.

4.3 Ablation studies

With all other hyperparameter choices kept constant, we vary the options regarding computation domain and the application of preconditioning, and summarize the outcome of model performance in Table 4. The combination of adopting logit domain computation without using preconditioning can sometimes increase the challenge in model convergence, and therefore, it is not recommended. The listed results on **Ego-small** and **Community-small** demonstrate that both techniques are in general beneficial for achieving better model

Table 4: The effect of practicing logit domain computation and preconditioning

logit domain	preconditioning	Ego-small				Community-small			
		Deg. ↓	Clus. ↓	Orbit. ↓	Avg. ↓	Deg. ↓	Clus. ↓	Orbit. ↓	Avg. ↓
-	-	0.015	0.018	0.004	0.012	0.010	0.076	0.004	0.030
-	✓	0.013	0.017	0.002	0.011	0.004	0.044	0.007	0.018
✓	✓	0.011	0.014	0.002	0.009	0.002	0.060	0.002	0.021

performance, and the effect of preconditioning is more evident when the computation is performed in the logit domain.

4.4 Visualization

We provide the visualization of the generative process and generated graphs of GBD in Appendix B. For generative process with general datasets shown in Appendix B.1, we follow the implementation described in Section 2.4 and the nodes in all adjacency matrices are reordered by decreasing node degree. Apparently, we can find that edges associated with nodes with large degree will be the first to be identified, and then spread in decreasing order of degree on both datasets. It’s worth noting that the reverse beta diffusion can converge rapidly, leading to generated graphs with correct topology at an early stage. This demonstrates that our proposed GBD can further explore the potential benefits of beta diffusion, resulting in valid graphs with stability and high quality. For generated molecule graphs shown in Appendix B.1, we can observe that GBD can successfully generate valid and high-quality 2D molecules, verifying its ability to model attributed graphs.

5 Conclusion, Limitations and Broader Impact

We introduce graph beta diffusion (GBD), a novel graph generation framework developed upon beta diffusion. We demonstrate that the utilization of beta distribution to define the diffusion process is beneficial for modeling the distribution of graph data, and outline four crucial designing elements—data transformation, concentration modulation, logit-domain computation, and neural-network precondition—that consistently enhance model performance.

With these contributions achieved, we identify several areas for potential improvement. First, while the beta distribution can adeptly model various data distributions within the range of $[0, 1]$, using it to construct the diffusion model necessitates careful selection of scaling and shifting parameters to ensure model convergence. This requirement can complicate the transfer of experience between different tasks. Second, unlike discrete diffusion processes, the beta diffusion process does not naturally generate discrete intermediate adjacency matrices for computing graph statistics. This necessitates a quantization strategy if one aims to incorporate statistics from these intermediates when predicting the graph at the initial state. Thirdly, diffusion-based graph generative models, including GBD, currently rely on a reverse diffusion process that takes hundreds to thousands of iterative refinement steps to generate a single sample. Recent advancements in score-based distillation techniques, originally developed for image diffusion models, could be adapted to distill the graph teacher model [Luo et al., 2023, Zhou et al., 2024]. Such an adaptation has the potential to significantly accelerate the graph generation process while maintaining or even improving performance. We plan to explore these possibilities in future studies.

Finally, we explore the potential impact of GBD. Since much real-world data can be structured as graphs, an effective tool for generating realistic graphs could significantly benefit researchers in the natural and social sciences, enabling the economical creation of high-quality simulated data. However, there is a concern: if the generated content is misused for fraudulent activities, distinguishing it from authentic data could become increasingly challenging for recipients.

References

- Emmanuel Abbe. Community detection and stochastic block models: recent developments. *Journal of Machine Learning Research*, 18(177):1–86, 2018.
- Edo M Airolidi, David Blei, Stephen Fienberg, and Eric Xing. Mixed membership stochastic blockmodels. In *Advances in Neural Information Processing Systems (NeurIPS)*, volume 21, 2009.
- Jacob Austin, Daniel D Johnson, Jonathan Ho, Daniel Tarlow, and Rianne Van Den Berg. Structured denoising diffusion models in discrete state-spaces. *Advances in Neural Information Processing Systems*, 34:17981–17993, 2021.
- Pavel Avdeyev, Chenlai Shi, Yuhao Tan, Kseniia Dudnyk, and Jian Zhou. Dirichlet diffusion score model for biological sequence generation. In *Proceedings of the Fortieth International Conference on Machine Learning*, Proceedings of Machine Learning Research. PMLR, 2023.
- Arindam Banerjee, Srujana Merugu, Inderjit S Dhillon, Joydeep Ghosh, and John Lafferty. Clustering with Bregman divergences. *Journal of machine learning research*, 6(10), 2005.
- Albert-László Barabási, Réka Albert, and Hawoong Jeong. Scale-free characteristics of random networks: the topology of the world-wide web. *Physica A: statistical mechanics and its applications*, 281(1-4):69–77, 2000.
- Guy W Bemis and Mark A Murcko. The properties of known drugs. 1. molecular frameworks. *Journal of medicinal chemistry*, 39(15):2887–2893, 1996.
- Pietro Bongini, Monica Bianchini, and Franco Scarselli. Molecular generative graph neural networks for drug discovery. *Neurocomputing*, 450:242–252, 2021.
- François Caron and Emily B Fox. Sparse graphs using exchangeable random measures. *Journal of the Royal Statistical Society Series B: Statistical Methodology*, 79(5):1295–1366, 2017.
- Tianqi Chen and Mingyuan Zhou. Learning to jump: Thinning and thickening latent counts for generative modeling. In *International Conference on Machine Learning*, pages 5367–5382. PMLR, 2023.
- Xiaohui Chen, Jiaying He, Xu Han, and Li-Ping Liu. Efficient and degree-guided graph generation via discrete diffusion modeling. In *International Conference on Machine Learning*. PMLR, 2023.
- Hyuna Cho, Minjae Jeong, Sooyeon Jeon, Sungsoo Ahn, and Won Hwa Kim. Multi-resolution spectral coherence for graph generation with score-based diffusion. In *Thirty-seventh Conference on Neural Information Processing Systems*, 2023.
- Valerio Ciotti, Ginestra Bianconi, Andrea Capocci, Francesca Colaiori, and Pietro Panzarasa. Degree correlations in signed social networks. *Physica A: Statistical Mechanics and its Applications*, 422:25–39, 2015.
- Marco Conti, Andrea Passarella, and Fabio Pezzoni. A model for the generation of social network graphs. In *2011 IEEE International Symposium on a World of Wireless, Mobile and Multimedia Networks*, pages 1–6. IEEE, 2011.
- Nicola De Cao and Thomas Kipf. Molgan: An implicit generative model for small molecular graphs. *arXiv preprint arXiv:1805.11973*, 2018.
- Vijay Prakash Dwivedi and Xavier Bresson. A generalization of transformer networks to graphs. *arXiv preprint arXiv:2012.09699*, 2020a.
- Vijay Prakash Dwivedi and Xavier Bresson. A generalization of transformer networks to graphs. *arXiv preprint arXiv:2012.09699*, 2020b.
- P ERDdS and A R&wi. On random graphs i. *Publ. math. debrecen*, 6(290-297):18, 1959.
- Paul Erdős, Alfréd Rényi, et al. On the evolution of random graphs. *Publ. math. inst. hung. acad. sci*, 5(1):17–60, 1960.

- Arthur Gretton, Karsten M Borgwardt, Malte J Rasch, Bernhard Schölkopf, and Alexander Smola. A kernel two-sample test. *The Journal of Machine Learning Research*, 13(1):723–773, 2012.
- Zhiye Guo, Jian Liu, Yanli Wang, Mengrui Chen, Duolin Wang, Dong Xu, and Jianlin Cheng. Diffusion models in bioinformatics and computational biology. *Nature reviews bioengineering*, 2(2):136–154, 2024.
- Kilian Konstantin Haefeli, Karolis Martinkus, Nathanaël Perraudin, and Roger Wattenhofer. Diffusion models for graphs benefit from discrete state spaces. In *The First Learning on Graphs Conference*, 2022.
- Xu Han, Xiaohui Chen, Francisco JR Ruiz, and Li-Ping Liu. Fitting autoregressive graph generative models through maximum likelihood estimation. *Journal of Machine Learning Research*, 24(97):1–30, 2023.
- Arman Hasanzadeh, Ehsan Hajiramezanali, Krishna Narayanan, Nick Duffield, Mingyuan Zhou, and Xiaoning Qian. Semi-implicit graph variational auto-encoders. In *Advances in Neural Information Processing Systems (NeurIPS)*, volume 32, pages 10711–10722, 2019.
- Yilin He, Chaojie Wang, Hao Zhang, Bo Chen, and Mingyuan Zhou. A variational edge partition model for supervised graph representation learning. *Advances in Neural Information Processing Systems*, 35:12339–12351, 2022.
- Jonathan Ho, Ajay Jain, and Pieter Abbeel. Denoising diffusion probabilistic models. *Advances in neural information processing systems*, 33:6840–6851, 2020.
- Paul W Holland, Kathryn Blackmond Laskey, and Samuel Leinhardt. Stochastic blockmodels: First steps. *Social networks*, 5(2):109–137, 1983.
- Han Huang, Leilei Sun, Bowen Du, and Weifeng Lv. Conditional diffusion based on discrete graph structures for molecular graph generation. In *NeurIPS 2022 Workshop on Score-Based Methods*, 2022.
- John J Irwin, Teague Sterling, Michael M Mysinger, Erin S Bolstad, and Ryan G Coleman. Zinc: a free tool to discover chemistry for biology. *Journal of chemical information and modeling*, 52(7):1757–1768, 2012.
- Wengong Jin, Regina Barzilay, and Tommi Jaakkola. Junction tree variational autoencoder for molecular graph generation. In *International conference on machine learning*, pages 2323–2332. PMLR, 2018.
- Jaehyeong Jo, Seul Lee, and Sung Ju Hwang. Score-based generative modeling of graphs via the system of stochastic differential equations. In *International Conference on Machine Learning*, pages 10362–10383. PMLR, 2022.
- Jaehyeong Jo, Dongki Kim, and Sung Ju Hwang. Graph generation with diffusion mixture. *arXiv preprint arXiv:2302.03596*, 2023.
- Tero Karras, Miika Aittala, Timo Aila, and Samuli Laine. Elucidating the design space of diffusion-based generative models. *Advances in Neural Information Processing Systems*, 35:26565–26577, 2022.
- Thomas N Kipf and Max Welling. Variational graph auto-encoders. *arXiv preprint arXiv:1611.07308*, 2016.
- Lingkai Kong, Jiaming Cui, Haotian Sun, Yuchen Zhuang, B Aditya Prakash, and Chao Zhang. Autoregressive diffusion model for graph generation. In *International Conference on Machine Learning*, pages 17391–17408. PMLR, 2023.
- Greg Landrum et al. Rdkit: Open-source cheminformatics, 2006.
- Clement Lee and Darren J Wilkinson. A review of stochastic block models and extensions for graph clustering. *Applied Network Science*, 4(1):1–50, 2019.
- Chen Li and Yoshihiro Yamanishi. Tengan: Pure transformer encoders make an efficient discrete gan for de novo molecular generation. In *International Conference on Artificial Intelligence and Statistics*, pages 361–369. PMLR, 2024.
- Yujia Li, Oriol Vinyals, Chris Dyer, Razvan Pascanu, and Peter Battaglia. Learning deep generative models of graphs. In *International conference on machine learning*. PMLR, 2018.

- Langzhang Liang, Zenglin Xu, Zixing Song, Irwin King, Yuan Qi, and Jieping Ye. Tackling long-tailed distribution issue in graph neural networks via normalization. *IEEE Transactions on Knowledge and Data Engineering*, 2023.
- Jenny Liu, Aviral Kumar, Jimmy Ba, Jamie Kiros, and Kevin Swersky. Graph normalizing flows. *Advances in Neural Information Processing Systems*, 32, 2019.
- Qi Liu, Miltiadis Allamanis, Marc Brockschmidt, and Alexander Gaunt. Constrained graph variational autoencoders for molecule design. *Advances in neural information processing systems*, 31, 2018.
- Weijian Luo, Tianyang Hu, Shifeng Zhang, Jiacheng Sun, Zhenguo Li, and Zhihua Zhang. Diff-Instruct: A universal approach for transferring knowledge from pre-trained diffusion models. In *Thirty-seventh Conference on Neural Information Processing Systems*, 2023. URL <https://openreview.net/forum?id=MLIs5iRq4w>.
- Youzhi Luo, Keqiang Yan, and Shuiwang Ji. Graphdf: A discrete flow model for molecular graph generation. In *International conference on machine learning*, pages 7192–7203. PMLR, 2021.
- Karolis Martinkus, Andreas Loukas, Nathanaël Perraudin, and Roger Wattenhofer. Spectre: Spectral conditioning helps to overcome the expressivity limits of one-shot graph generators. In *International Conference on Machine Learning*, pages 15159–15179. PMLR, 2022.
- Nikhil Mehta, Lawrence Carin, and Piyush Rai. Stochastic blockmodels meet graph neural networks. In *International Conference on Machine Learning (ICML)*, pages 4466–4474, 2019.
- Mark EJ Newman, Duncan J Watts, and Steven H Strogatz. Random graph models of social networks. *Proceedings of the national academy of sciences*, 99(suppl_1):2566–2572, 2002.
- Chenhao Niu, Yang Song, Jiaming Song, Shengjia Zhao, Aditya Grover, and Stefano Ermon. Permutation invariant graph generation via score-based generative modeling. In Silvia Chiappa and Roberto Calandra, editors, *Proceedings of the Twenty Third International Conference on Artificial Intelligence and Statistics*, volume 108 of *Proceedings of Machine Learning Research*, pages 4474–4484. PMLR, 26–28 Aug 2020a.
- Chenhao Niu, Yang Song, Jiaming Song, Shengjia Zhao, Aditya Grover, and Stefano Ermon. Permutation invariant graph generation via score-based generative modeling. In *International Conference on Artificial Intelligence and Statistics*, pages 4474–4484. PMLR, 2020b.
- Adam Paszke, Sam Gross, Francisco Massa, Adam Lerer, James Bradbury, Gregory Chanan, Trevor Killeen, Zeming Lin, Natalia Gimelshein, Luca Antiga, et al. Pytorch: An imperative style, high-performance deep learning library. *Advances in neural information processing systems*, 32, 2019.
- Raghunathan Ramakrishnan, Pavlo O Dral, Matthias Rupp, and O Anatole Von Lilienfeld. Quantum chemistry structures and properties of 134 kilo molecules. *Scientific data*, 1(1):1–7, 2014.
- Prithviraj Sen, Galileo Namata, Mustafa Bilgic, Lise Getoor, Brian Galligher, and Tina Eliassi-Rad. Collective classification in network data. *AI magazine*, 29(3):93–93, 2008.
- Chence Shi, Minkai Xu, Zhaocheng Zhu, Weinan Zhang, Ming Zhang, and Jian Tang. Graphaf: a flow-based autoregressive model for molecular graph generation. In *International Conference on Learning Representations*, 2020.
- Pouyan Shirzadian, Blessy Antony, Akshaykumar G Gattani, Nure Tasnina, and Lenwood S Heath. A time evolving online social network generation algorithm. *Scientific Reports*, 13(1):2395, 2023.
- Martin Simonovsky and Nikos Komodakis. Graphvae: Towards generation of small graphs using variational autoencoders. In *Artificial Neural Networks and Machine Learning–ICANN 2018: 27th International Conference on Artificial Neural Networks, Rhodes, Greece, October 4-7, 2018, Proceedings, Part I 27*, pages 412–422. Springer, 2018.
- Jascha Sohl-Dickstein, Eric Weiss, Niru Maheswaranathan, and Surya Ganguli. Deep unsupervised learning using nonequilibrium thermodynamics. In *International conference on machine learning*, pages 2256–2265. PMLR, 2015.

- Yang Song and Stefano Ermon. Generative modeling by estimating gradients of the data distribution. *Advances in neural information processing systems*, 32, 2019.
- Yang Song, Jascha Sohl-Dickstein, Diederik P Kingma, Abhishek Kumar, Stefano Ermon, and Ben Poole. Score-based generative modeling through stochastic differential equations. In *International Conference on Learning Representations*, 2021.
- Clement Vignac, Igor Krawczuk, Antoine Siraudin, Bohan Wang, Volkan Cevher, and Pascal Frossard. Digress: Discrete denoising diffusion for graph generation. In *The Eleventh International Conference on Learning Representations*, 2023.
- Haohui Wang, Baoyu Jing, Kaize Ding, Yada Zhu, Liqing Zhang, and Dawei Zhou. Characterizing long-tail categories on graphs. *arXiv preprint arXiv:2305.09938*, 2023.
- Hongwei Wang, Jia Wang, Jialin Wang, Miao Zhao, Weinan Zhang, Fuzheng Zhang, Xing Xie, and Minyi Guo. Graphgan: Graph representation learning with generative adversarial nets. In *Proceedings of the AAAI conference on artificial intelligence*, volume 32, 2018.
- Jiaxuan You, Rex Ying, Xiang Ren, William Hamilton, and Jure Leskovec. Graphrnn: Generating realistic graphs with deep auto-regressive models. In *International conference on machine learning*, pages 5708–5717. PMLR, 2018.
- Chengxi Zang and Fei Wang. Moflow: an invertible flow model for generating molecular graphs. In *Proceedings of the 26th ACM SIGKDD international conference on knowledge discovery & data mining*, pages 617–626, 2020.
- Mingyuan Zhou. Infinite edge partition models for overlapping community detection and link prediction. In *International Conference on Artificial Intelligence and Statistics (AISTATS)*, volume 38 of *Proceedings of Machine Learning Research*, pages 1135–1143, 2015.
- Mingyuan Zhou, Tianqi Chen, Zhendong Wang, and Huangjie Zheng. Beta diffusion. In *NeurIPS 2023: Neural Information Processing Systems*, 2023.
- Mingyuan Zhou, Huangjie Zheng, Zhendong Wang, Mingzhang Yin, and Hai Huang. Score identity distillation: Exponentially fast distillation of pretrained diffusion models for one-step generation. In *International Conference on Machine Learning*, 2024.

A Experimental Details

A.1 General graph generation

Datasets We evaluated our model using three synthetic and real datasets of varying size and connectivity, previously used as benchmarks in the literature [Cho et al., 2023, Jo et al., 2022]: **Ego-small** [Sen et al., 2008] consists of 200 small real sub-graphs from the Citeseer network dataset with $4 \leq N \leq 18$. **Community-small** consists of 100 randomly generated synthetic graphs with $12 \leq N \leq 20$, where the graphs are constructed by two equal-sized communities, each of which is generated by the Erdős–Rényi model [Erdős et al., 1960], with $p = 0.7$ and $0.05N$ inter-community edges are added with uniform probability as in previous works [Jo et al., 2022, Niu et al., 2020b]. **Grid** consists of randomly generated 100 standard 2D grid graphs with $100 \leq N \leq 400$ and the maximum number of edges per node is 4 since all nodes are arranged in a regular lattice.

Evaluation metrics For a fair comparison, we follow the experimental and evaluation settings of Jo et al. [2022, 2023], using the same train/test split, where 80% of the data is used as the training set and the remaining 20% as the test set. We adopt maximum mean discrepancy (MMD) as our evaluation metric to compare three graph property distributions between test graphs and the same number of generated graphs: degree (**Deg.**), clustering coefficient (**Clus.**), count of orbits with 4 nodes (**Orbit**) and their average score (**Avg.**). Note that we use the Gaussian Earth Mover’s Distance (EMD) kernel to compute the MMDs following the method used in previous work [Jo et al., 2022, Cho et al., 2023].

Implementation details We follow the evaluation setting of Jo et al. [2022], Cho et al. [2023] to generate graphs of the same size as the test data in each run and we report the mean and standard deviation obtained from 3 independent runs for each dataset. We report the baseline results taken from Cho et al. [2023], except for the results of ConGress in Tables 1 and 2, which we obtained by running its corresponding open-source code. For a fair comparison, we adopt the Graph Transformer [Dwivedi and Bresson, 2020b, Vignac et al., 2023] as the neural network used in GDSS+Transformer [Jo et al., 2022], DiGress [Vignac et al., 2023], and DruM [Jo et al., 2023]. We set the diffusion steps to 1000 for all the diffusion models. For important hyperparameters mentioned in Sec 2.4, we usually set $S_{scale} = 0.9$, $S_{hift} = 0.09$. and $\eta = [10000, 100, 30, 10]$ for the normalized degrees corresponding to the intervals falling in the interval split by $[1.0, 0.8, 0.4, 0.1]$, respectively. In practice, we set threshold as 0.9 to quantize generated continue adjacency matrix.

A.2 2D molecule generation

Datasets We utilize two widely-used molecular datasets as benchmarks, as described in Jo et al. [2023]: **QM9** [Ramakrishnan et al., 2014], consisting of 133,885 molecules with $N \leq 9$ nodes from 4 different node types and **ZINC250k** [Irwin et al., 2012], consisting of 249,455 molecules with $N \leq 38$ nodes from 9 node types. Molecules in both datasets have 3 edge types, namely single bond, double bond, and triple bond. Following the standard procedure in the literature [Shi et al., 2020, Luo et al., 2021, Jo et al., 2022, 2023], we kekulize the molecules using the RDKit library [Landrum et al., 2006] and remove the hydrogen atoms from the molecules in the QM9 and ZINC250k datasets.

Evaluation metrics Following the evaluation setting of Jo et al. [2022], we generate 10,000 molecules for each dataset and evaluate them with four metrics: the ratio of valid molecules without correction (**Val.**). Frechet ChemNet Distance (**FCD**) evaluates the chemical properties of the molecules by measuring the distance between the feature vectors of generated molecules and those in the test set using ChemNet. Neighborhood Subgraph Pairwise Distance Kernel (**NSPDK**) assesses the quality of the graph structure by measuring the MMD between the generated molecular graphs and the molecular graphs from the test set. Scaffold Similarity (**Scaf.**) evaluates the ability to generate similar substructures by measuring the cosine similarity of the frequencies of Bemis-Murcko scaffolds [Bemis and Murcko, 1996].

Implementation details We follow the evaluation setting of Jo et al. [2022, 2023] to generate 10,000 molecules and evaluate graphs with test data for each dataset. We quote the baselines results from Jo et al. [2023]. For a fair comparison, we adopt the Graph Transformer [Dwivedi and Bresson, 2020b, Vignac et al., 2023] as the neural network used in GDSS+Transformer [Jo et al., 2022], DiGress [Vignac et al., 2023], and DruM [Jo et al., 2023]. We apply the exponential moving average (EMA) to the parameters while sampling and set the diffusion steps to 1000 for all the diffusion models. For both QM9 and ZINC250k, we encode nodes and edges to one-hot and set $S_{scale} = 0.9$, $S_{shift} = 0.09$. For η modulated in molecule generation, with the help of chemical knowledge, we apply $\eta = [10000, 100, 100, 100, 30]$ on carbon-carbon bond, carbon-nitrogen, carbon-oxygen, carbon-fluorine, and other possible bonds, respectively. For η of nodes, we apply $\eta = [10000, 100, 100, 30]$ on carbon atom, nitrogen atom, oxygen atom and other possible atoms, respectively. As described in Sec 2.4, applying appropriate η for different node types and edge types can prolong the presence of related substructures during the diffusion process. In practice, we set threshold as 0.9 to quantize generated continue adjacency matrix and the value in discrete adjacency matrix is 0 after quantizing if and only if all values in each dimension are all 0.

A.3 Computing resources

For all experiments, we utilized the PyTorch [Paszke et al., 2019] framework to implement GBD and trained the model with NVIDIA GeForce RTX 4090 and RTX A5000 GPUs.

B Visualization

B.1 Generative process of GBD on general datasets

We visualize generative process of GBD on the **Community-small** and the **Ego-small** dataset in Figures 3 and 4, respectively.

B.2 Generated graphs of GBD on 2D molecule datasets

We provide the visualization of the 2D molecules generated by GBD on the **QM9** and the **ZINC250k** datasets in Figure 5 and in Figure 6, respectively.

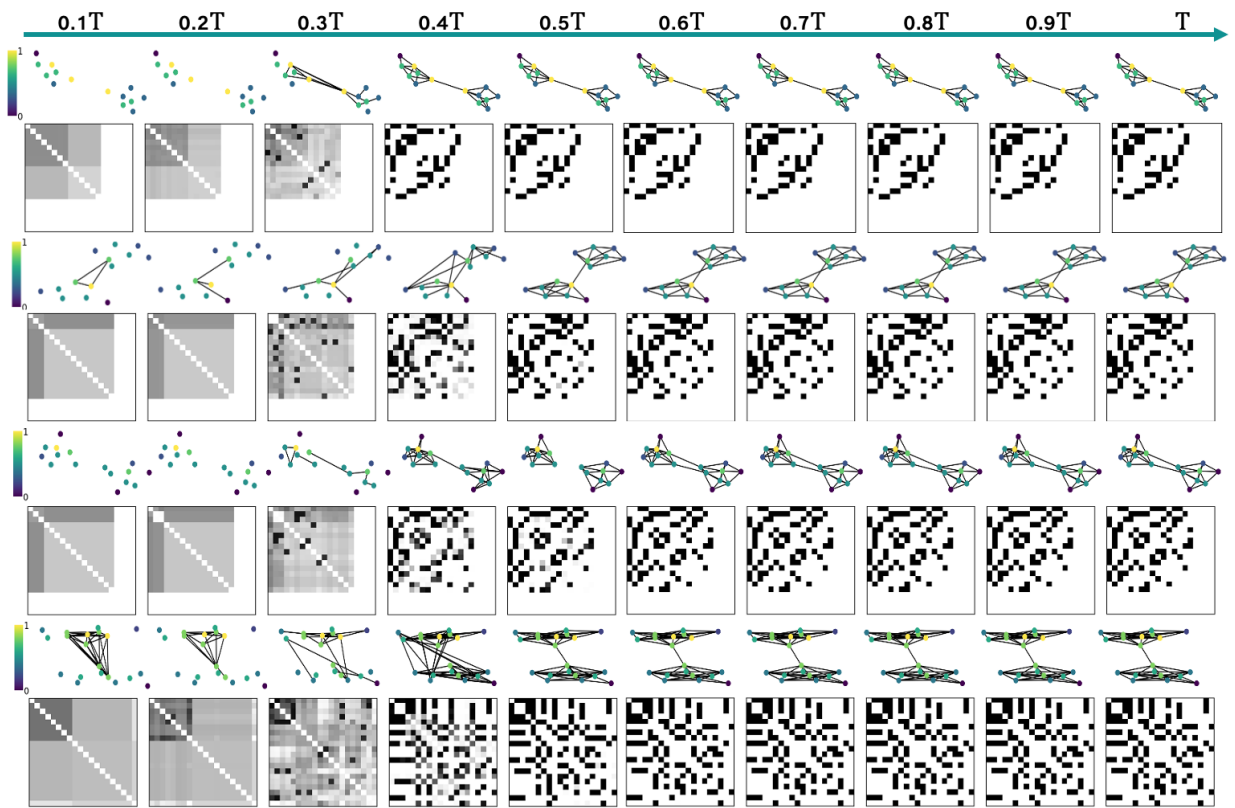


Figure 3: Visualization of the generative process of GBD on the **Community-small** dataset.

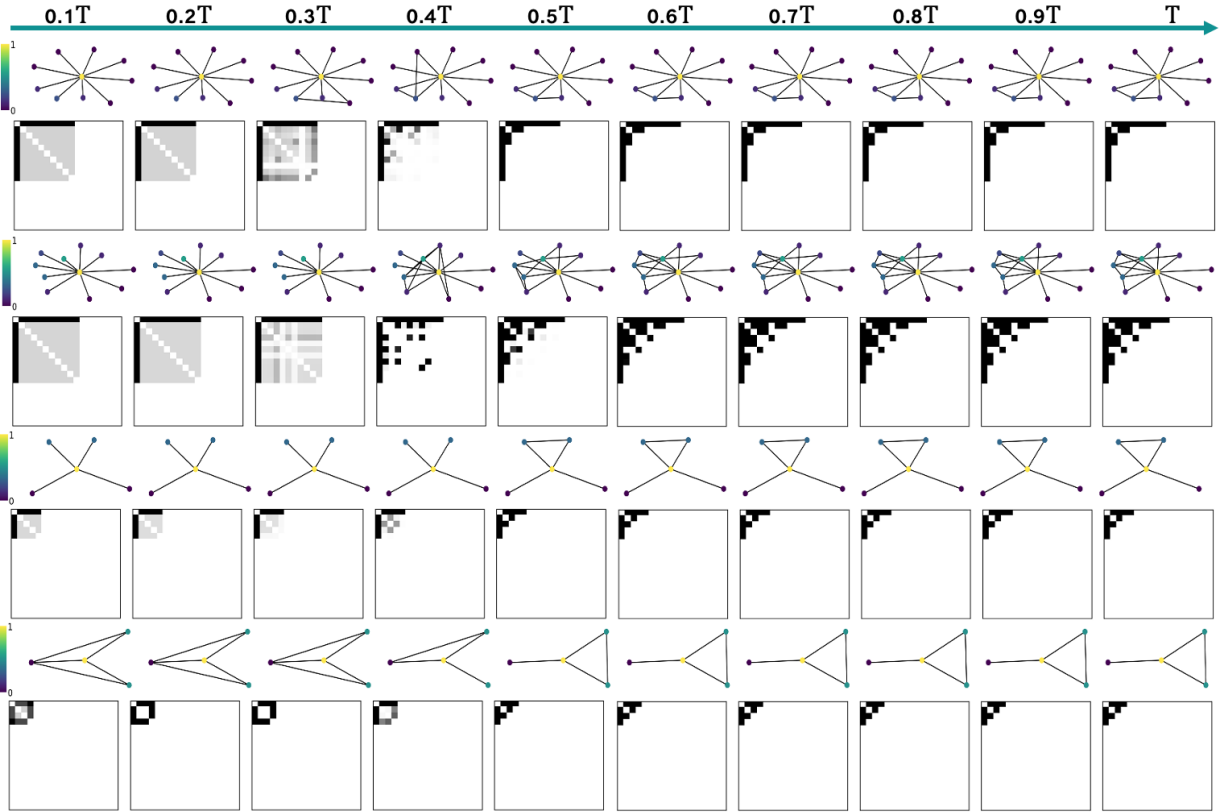


Figure 4: Visualization of the generative process of GBD on the **Ego-small** dataset.

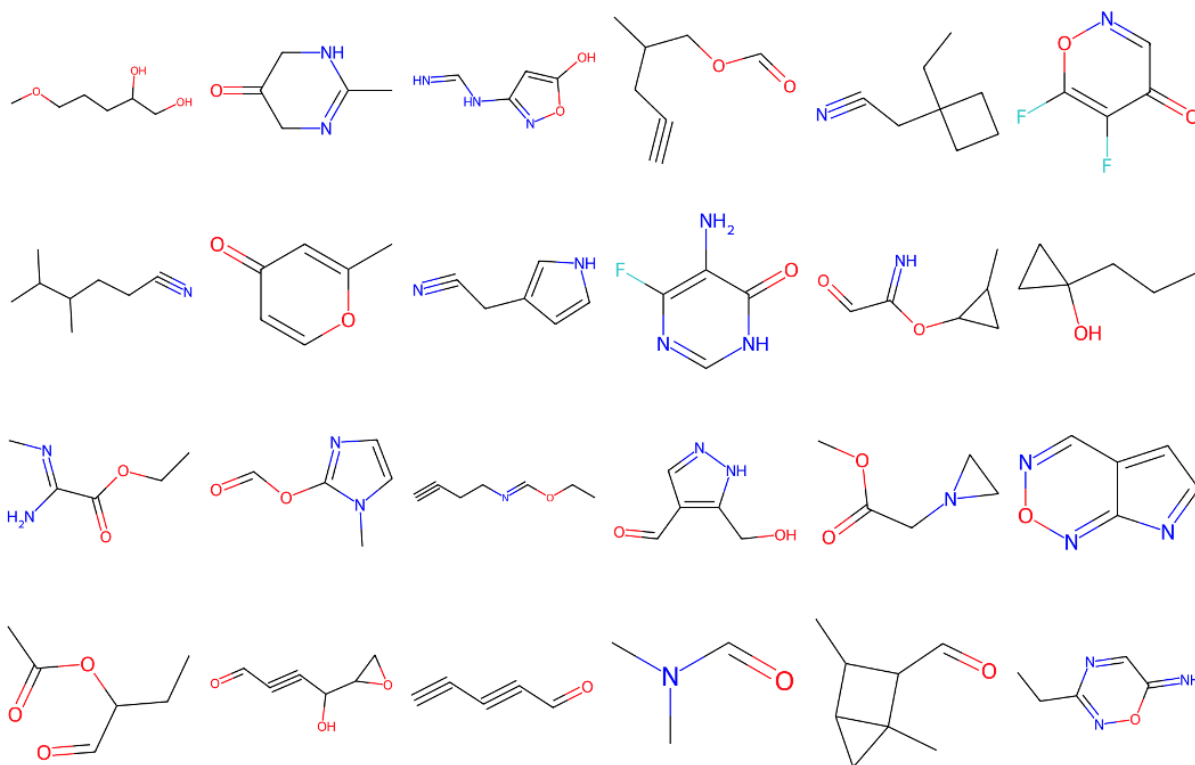


Figure 5: Visualization of the generated graphs of GBD on the **QM9** dataset.

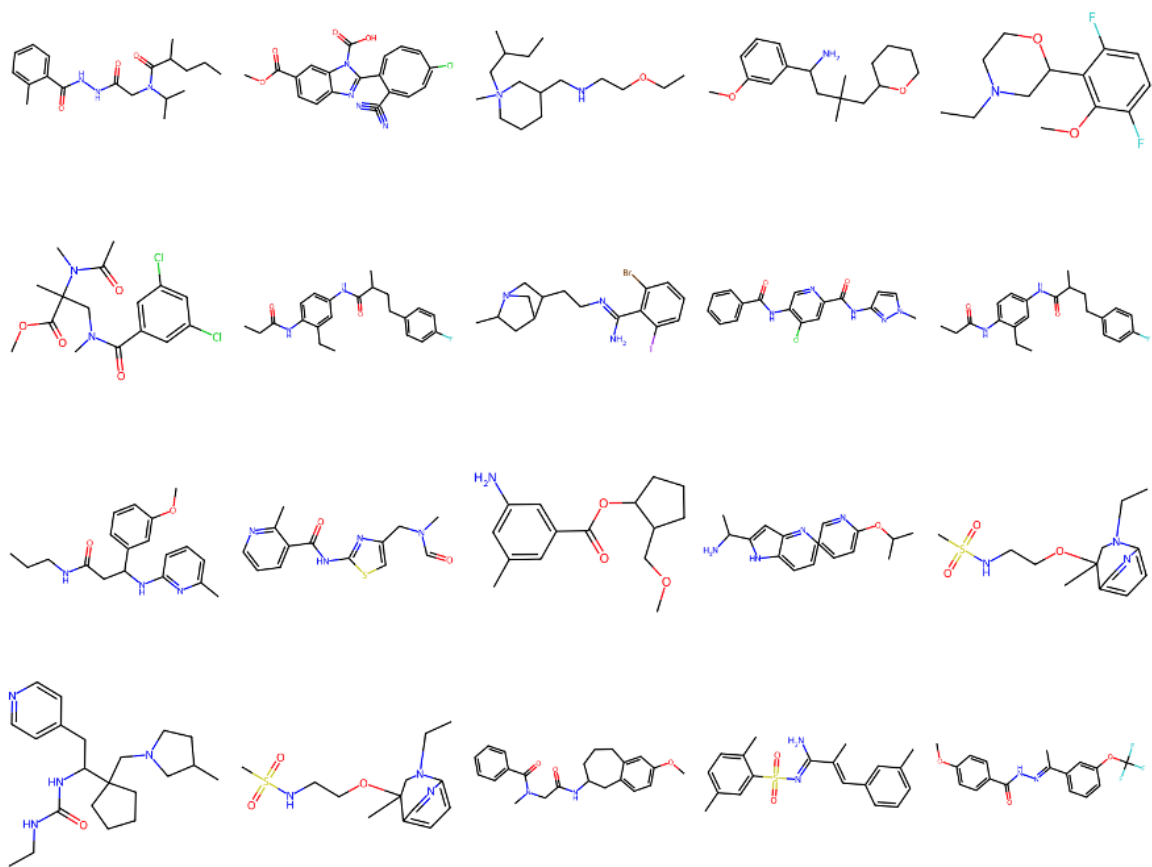


Figure 6: Visualization of the generative process of GBD on the **ZINC250k** dataset.